

Research Article

Pepper catalase: a broad analysis of its modulation during fruit ripening and by nitric oxide

Salvador González-Gordo¹, Javier López-Jaramillo², Marta Rodríguez-Ruiz¹, Jorge Taboada¹, José M. Palma¹ and  Francisco J. Corpas¹

¹Group of Antioxidants, Free Radicals and Nitric Oxide in Biotechnology, Food and Agriculture, Department of Stress, Development and Signaling in Plants, Estación Experimental del Zaidín, Spanish National Research Council (CSIC), Profesor Albareda 1, E-18008 Granada, Spain Granada, Spain; ²Instituto de Biotecnología, Universidad de Granada, 18003 Granada, Spain

Correspondence: Francisco J. Corpas (javier.corpas@eez.csic.es)



Catalase is a major antioxidant enzyme located in plant peroxisomes that catalyzes the decomposition of H_2O_2 . Based on our previous transcriptomic (RNA-Seq) and proteomic (iTRAQ) data at different stages of pepper (*Capsicum annuum* L.) fruit ripening and after exposure to nitric oxide (NO) enriched atmosphere, a broad analysis has allowed us to characterize the functioning of this enzyme. Three genes were identified, and their expression was differentially modulated during ripening and by NO gas treatment. A dissimilar behavior was observed in the protein expression of the encoded protein catalases (CaCat1–CaCat3). Total catalase activity was down-regulated by 50% in ripe (red) fruits concerning immature green fruits. This was corroborated by non-denaturing polyacrylamide gel electrophoresis, where only a single catalase isozyme was identified. *In vitro* analyses of the recombinant CaCat3 protein exposed to peroxynitrite ($ONOO^-$) confirmed, by immunoblot assay, that catalase underwent a nitration process. Mass spectrometric analysis identified that Tyr348 and Tyr360 were nitrated by $ONOO^-$, occurring near the active center of catalase. The data indicate the complex regulation at gene and protein levels of catalase during the ripening of pepper fruits, with activity significantly down-regulated in ripe fruits. Nitration seems to play a key role in this down-regulation, favoring an increase in H_2O_2 content during ripening. This pattern can be reversed by the exogenous NO application. While plant catalases are generally reported to be tetrameric, the analysis of the protein structure supports that pepper catalase has a favored quaternary homodimer nature. Taken together, data show that pepper catalase is down-regulated during fruit ripening, becoming a target of tyrosine nitration, which provokes its inhibition.

Introduction

Pepper belongs to the Solanaceae, a family that harbors other horticultural species like tomatoes, eggplant, or potatoes. Pepper is a crop with great economic relevance since its fruits are one of the most consumed horticultural products worldwide either raw, cooked, or in powdered form as spice or colorant [1,2]. At a nutritional level, pepper fruit is a relevant source of vitamins (A, C, and E), flavonoids, fiber, and minerals [3]. Available data support that during ripening pepper fruits undergo an active metabolism of reactive oxygen and nitrogen species (ROS and RNS, respectively) where multiple enzymatic components are regulated at different levels (activity, gene, and protein expression) [4–9]. Likewise, other related actors such as small heat shock proteins, NADPH, and hydrogen sulfide-generating enzymes are also influenced by fruit ripening [10–14].

Catalase (EC 1.11.1.6) is a key H_2O_2 -scavenging enzyme and the main antioxidant and constitutive enzyme located in the matrix of the peroxisomes while there is an ascorbate peroxidase (APX) linked to the membrane of this organelle [15]. In fact, catalase was set as a marker of peroxisomes by the

Received: 22 May 2024
 Revised: 13 June 2024
 Accepted: 17 June 2024

Accepted Manuscript online:
 17 June 2024
 Version of Record published:
 3 July 2024

pioneer studies of Professor De Duve's group [16,17]. In higher plants, catalases are encoded by a multigene family [18–22] and, consequently, plants are able to contain several isozymes which could be either constitutively expressed or induced under certain physiological or environmental conditions [23–31]. Thus, catalase activity is one of the first lines of defense against both abiotic and biotic stresses that are usually accompanied by oxidative stress conditions [32–39]. However, it must always be taken into consideration that plants have a large array of enzymatic and non-enzymatic antioxidant systems present in various subcellular compartments that can remove H_2O_2 directly or indirectly such as APX, glutathione peroxidases, ascorbate, flavonoids or via the Fenton reaction, among others. These systems must function in a co-ordinated manner both under physiological conditions, such as seed germination, root development, leaf growth, and fruit ripening, and in response to adverse environmental conditions.

Nitric oxide (NO; nitrogen monoxide) is a free radical because its N atom has an unpaired electron in its π orbital, but it could undergo a one-electron oxidation or reduction to generate nitrosonium cation (NO^+) or nitroxyl anion (NO^-), respectively. Additionally, NO has other derived molecules named RNS such as S-nitrosogluthathione (GSNO), peroxyxynitrite ($ONOO^-$), and nitric dioxide (NO_2), among others. Although the enzymatic source of NO is still controversial in higher plants [40,41], the relevance of NO as a signal molecule has been shown in almost all of the physiological and stressful processes where its metabolism has been studied. Many of the regulatory functions attributed to NO are exerted through protein posttranslational modifications (PTMs), mainly tyrosine nitration, S-nitrosation, and metal nitrosylation [42], as well as by its cross-talk with other molecules including phytohormones and, more recently, with hydrogen sulfide (H_2S) [43].

During fruit postharvest storage, catalase activity has been shown to be positively modulated by exogenous molecules such as NO [44,45], H_2S or melatonin [46], thus contributing to maintaining fruit quality. In previous studies, we have shown some atypical biochemical characteristics of the catalase enzyme from sweet pepper fruit [47–49]; however, many questions such as the number the catalase genes and their expression during fruit ripening are still unanswered. This study aims to provide a broad analysis of pepper catalase during the ripening of pepper fruit and under an enriched NO atmosphere. Overall, the data provide a differential modulation in activity, protein, and gene expression of the three identified *catalase* genes, as well as a mass spectrometry (MS) analysis which has allowed us to understand why catalase is a dimer in pepper fruit and to identify that the enzyme undergoes protein tyrosine nitration in this plant material. Additionally, this NO-derived PTM is a candidate to justify the down-regulation undergone by the catalase activity in ripe pepper fruits.

Results

Identification and characterization of the *catalase* (CAT) genes in pepper fruits

The analysis of the available catalase sequences from several plant species, and the mining of the *Capsicum annuum* L. genome allowed the identification of three *CAT* genes, designated *CaCAT1* to *CaCAT3*, according to their chromosomal distribution in chromosomes (Chr.) 2, 4, and 12, respectively. Table 1 recapitulates some properties of these genes and their corresponding encoded catalase proteins including the number of amino acids (aa), and molecular mass (kDa). At the protein level, Cat1 shares identities of 78.3% and 79.5% with Cat2 and Cat3, respectively, whereas Cat2 and Cat3 share an identity of 85.8%.

The genomic analyses of the *CaCAT* genes indicated that the three genes contain 8 exons and 7 introns with different lengths, and *CaCAT3* has the longest intron of ~2000 nucleotides. The total length of the three genes is ~5000 nucleotides (Figure 1).

Table 1. Sweet pepper genes encoding different peroxisomal catalases.

Gene	Gene ID	Chr.	Genomic location	Protein ID	Length (aa)	Mw (kDa)	pI
CAT 1	107859787	2	137235722–137239921	XP_016560382.1	492	56.92	6.73
CAT 2	107866793	4	230684242–230689087	NP_001311851.1	492	56.92	7.72
CAT 3	107850312	12	223373959–223378669	NP_001311603.1	492	56.48	7.05

Protein length in amino acids (aa) corresponds to the pre-processed polypeptides. Theoretical pI and molecular weight (Mw) of each mature protein were predicted *in silico* using the Compute pI/Mw tool on the Expasy server.

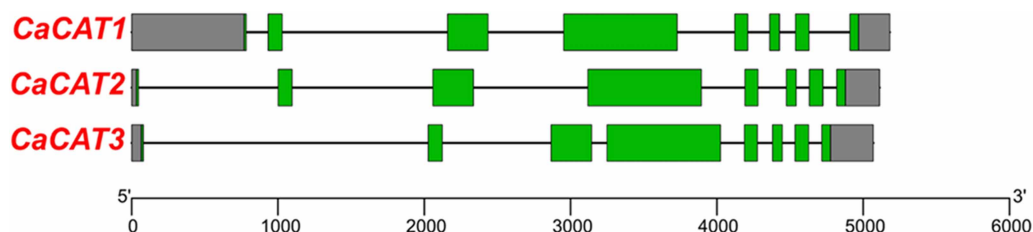


Figure 1. Structure of the three pepper fruit *CaCAT* genes.

Untranslated regions are presented in gray boxes, exons in green boxes, and introns with black lines. Exon–intron regions are represented in scale.

The analysis of the upstream region (1500 bp) from the transcription starting point of the three *CaCAT* genes allows identifying the presence of 15 cis-regulatory elements (CREs) involved in three main processes including light responsive, stress, and phytohormones. Among these CREs, the G-box seems to exert a higher effect on *CaCAT2*. Supplementary Figure S1 illustrates the heatmap of these 15 identified CREs.

CAT gene and protein expression, and activity during pepper fruit ripening and under exogenous NO gas treatment

The time-course expression analyses by RNAseq of the three *CaCAT* genes throughout fruit ripening and after NO gas treatment are presented in Figure 2. The ripening stages correspond to immature green (G) fruit, breaking point 1 (BP1), breaking point 2 with and without NO treatment (BP2 + NO and BP2 – NO, respectively), and ripe red (R) fruit (see Supplementary Figure S2). During ripening, *CaCAT1* and *CaCAT3* were both down-regulated, whereas *CaCAT2* was up-regulated. On the other hand, the exogenous NO treatment of fruits triggered a significant increase in the expression of *CaCAT1*, whereas *CaCAT2* showed a slight but no significant increase and *CaCAT3* was unaffected.

The protein expression analysis was accomplished using the proteomes obtained by iTRAQ in the same stages described in Figure 2. Thus, the three *CaCat* isoforms were identified in all the analyzed proteomes and their comparative analyses are shown in Figure 3. Thus, the upper panels illustrate that the expression of *Cat1* increased slightly but not significantly in ripe red fruits with respect to green ones. However, *Cat2* and *Cat3*

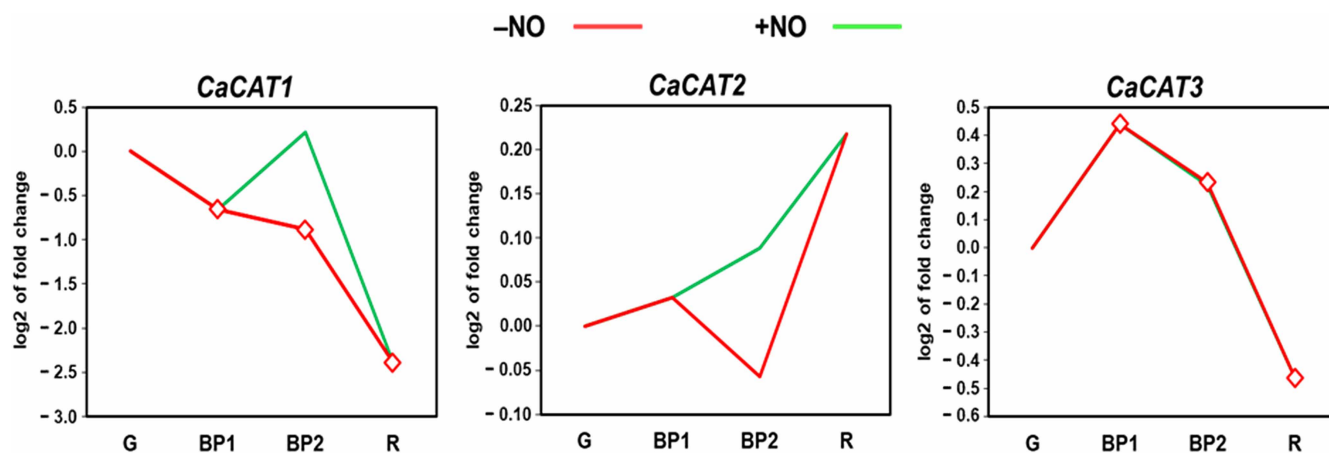


Figure 2. Time-course expression analysis by RNAseq of the three *CaCAT* genes during fruit ripening conditions and after exogenous NO treatment.

Pepper fruit samples were selected at different ripening stages including immature green (G), breaking point 1 (BP1), breaking point 2 with (green line) and without (red line) NO treatment (BP2 + NO and BP2 – NO, respectively) and ripe red (R). The green line corresponds to BP2 fruits treated with NO whereas the red line corresponds to untreated fruits. Statistically significant changes in expression levels ($P < 0.05$) compared with green fruit (G) are indicated with diamonds.

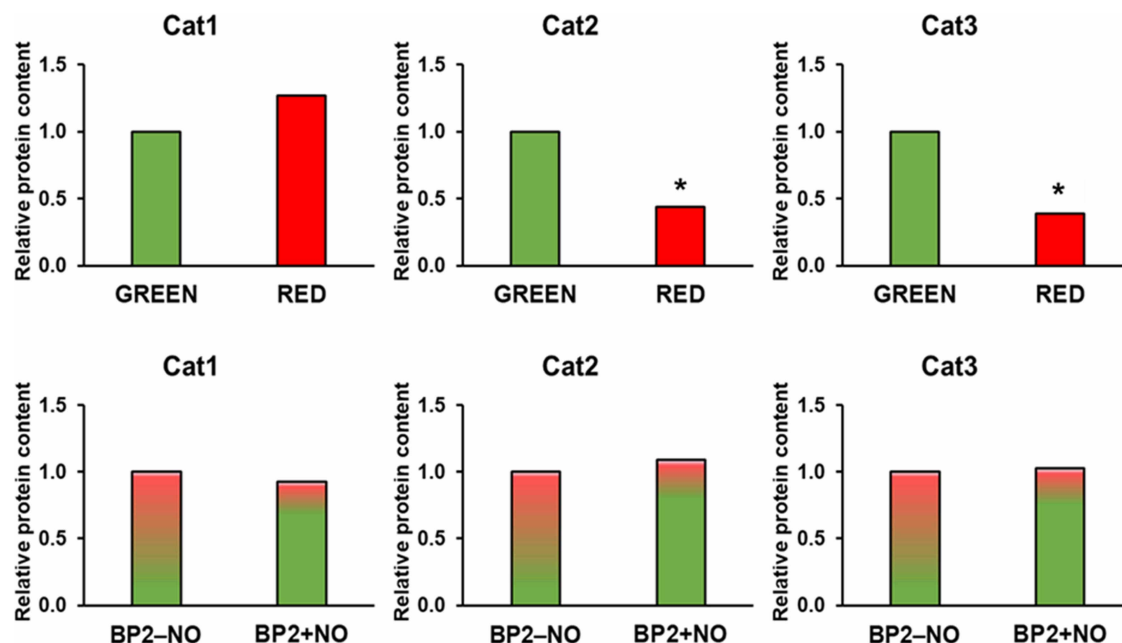


Figure 3. Time-course expression analysis by iTRAQ of the three identified CaCat proteins throughout pepper fruit ripening (upper panels) and exposed to NO gas (lower panels).

The different stages correspond to immature green fruits, breaking point 1 (BP1), and breaking point 2 with and without NO treatment (BP2 + NO and BP2 – NO, respectively), and ripe red fruits. Asterisks for CaCat2 and CaCat3 indicate that differences were statistically significant ($P < 0.05$) in comparison with green fruits.

expression significantly decreased ~3-fold. On the other hand, a comparative analysis of the expression of these three catalase isozymes after the NO treatment was also performed, but the protein expression of any of the Cat isozymes was significantly affected (Figure 3, lower panels).

Figure 4 shows the spectrophotometric analysis of the total catalase activity during fruit ripening and under NO treatments. Once the ripening process is initiated (BP1), catalase activity increases, but in ripe red fruits, the activity decreases by 50%. On the other hand, the NO gas treatment seems to exert a positive effect on the catalase activity (BP2 + NO). Complementary, the catalase activity was also analyzed by non-denaturing PAGE. Figure 5a,b illustrates the presence of a single catalase band in all the analyzed stages and its relative quantification, respectively. The catalase activity was 3-fold diminished in the red fruits in comparison with the green ones; however, NO treatment (BP + NO) had no effect in comparison with untreated fruits at the BP2 stage (BP – NO).

Nitration of the catalase protein

To get deeper insights into the pepper catalase regulation, recombinant Cat3 protein was obtained by sequencing the pepper clone and overexpressing it in yeast. Figure 6a,b shows the SDS-PAGE analysis of the recombinant purified Cat3 proteins obtained after LYTRAP affinity column chromatography and its corresponding immunoblot probed with antibody against its 6xHis tag, respectively. Thus, a single band of ~58 kDa was obtained which is in good agreement to the expected theoretical molecular mass of 56.48 kDa of the catalase protein plus the 1.55 kDa corresponding to the 10xHis tag (0.93 kDa). Unfortunately, the obtained recombinant Cat3 was not enzymatically active, so its specific activity could not be tested against any potential NO donor. Alternatively, immunoblot assays using an antibody against nitrotyrosine (NO₂-Tyr) were carried out. Thus, the recombinant CaCat3 protein was incubated with increasing concentrations of SIN-1 (0, 0.5, 1, 2, and 5 mM) previous to SDS-PAGE and then analyzed by immunoblot assay with the antibody against NO₂-Tyr. Figure 6c shows an immunoreactive band of 58 kDa, detected after pre-incubation of the recombinant catalase with 0.5–5.0 mM SIN-1.

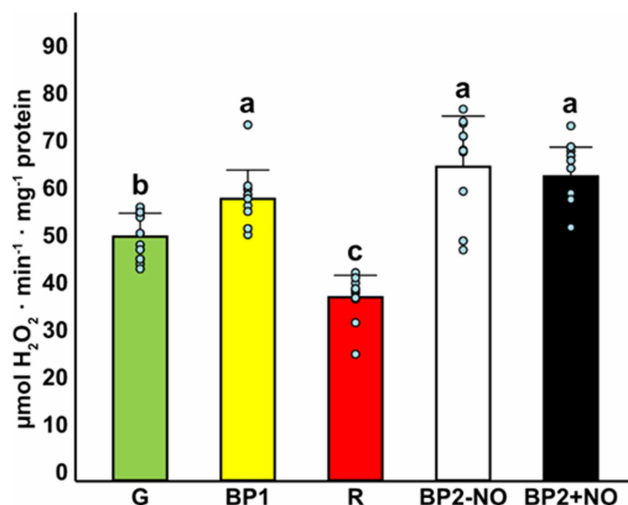
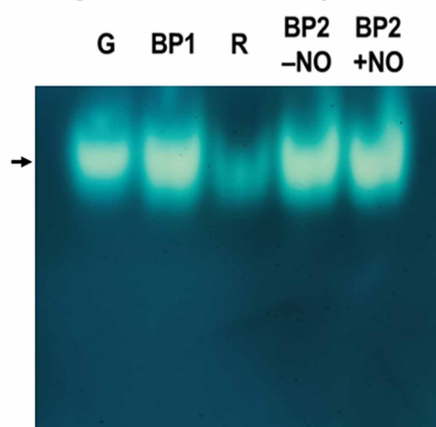


Figure 4. Spectrophotometric analysis of catalase activity from sweet pepper fruits at different ripening stages and exposed to NO gas.

Samples correspond to immature green (G) fruit, breaking point 1 (BP1), breaking point 2 with and without NO treatment (BP2 + NO and BP2 – NO, respectively), and ripe red (R). Data are means ± SEM of three independent biological samples. Different letters indicate that the differences among means are statistically significant ($P < 0.05$).

To identify which of the 20 Tyr present in the pepper catalase protein is(are) target(s) of the nitration event, non-nitrated and ONOO⁻-treated recombinant catalase were subjected to trypsin digestion followed by matrix-assisted laser desorption/ionization-time-of-flight (MALDI-TOF/TOF) MS examination (Figure 7a,b). Among the identified peptides, two of them containing nitrated tyrosines within the catalase amino acid sequences IGPNYMQLPVNAPK and HRIGPNYMQLPVNAPK with masses of 1585.792 Da (1541.813 + 44.985 Da) and 1894.947 Da (1849.962 + 44.985 Da) were compatible with the acquisition of a nitro (–NO₂) group (–NO₂ mass: 44.985 Da) on Tyr348 and Tyr360, respectively.

(a) In-gel catalase activity



(b) Relative quantification

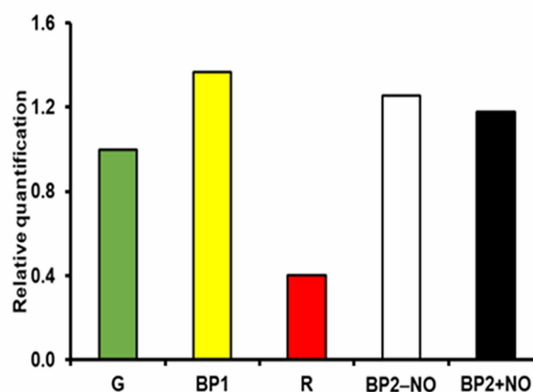


Figure 5. Catalase activity staining in non-denaturing polyacrylamide gel electrophoresis of sweet pepper fruits at different stages of ripening and exposed to NO gas: immature green (G), breaking point 1 (BP1), breaking point 2 with and without NO treatment (BP2 + NO and BP2 – NO, respectively), and ripe red (R).

(A) Representative picture of a gel stained for catalase activity. (B) Relative quantification of the band activity was determined using ImageJ software.

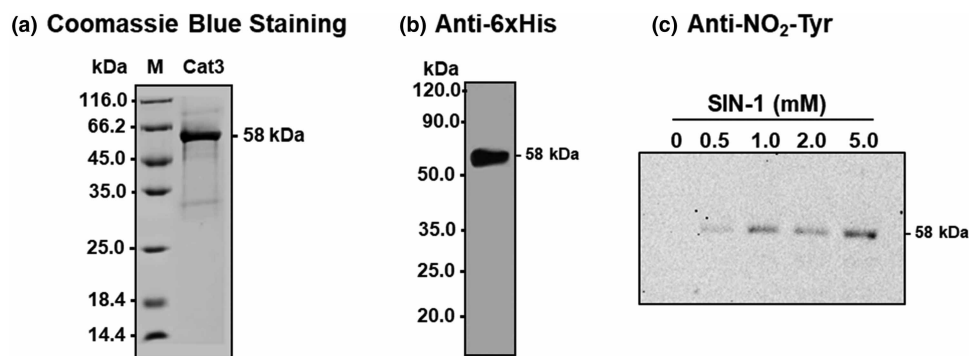


Figure 6. SDS-PAGE (15% acrylamide) and immunoblot analyses of recombinant purified pepper catalase.

(a) Coomassie blue staining of the N-terminal 10x His-tagged CaCat3 after affinity purification by immobilized metal affinity chromatography. (b) Recombinant CaCat3 was probed with a mouse anti-6xHis monoclonal antibody (dilution 1:2000). (c) Representative immunoblot showing the degree of tyrosine nitration of recombinant CaCat3 treated with different concentrations of SIN-1, as peroxynitrate donor, and detected with an antibody against 3-nitrotyrosine (dilution 1:2000). For protein staining, 4 μ g protein was used and 15 ng for immunoblot assay.

Modeling of the pepper catalase

The 3D structure of the catalase from *C. annuum* was modeled by submitting the primary structure to different servers. The rationale behind this strategy is that, although most algorithm relies on homology modeling, the selection of the template, coverage (i.e. percentage of the primary structure modeled), and the modeling of the poor-homology regions is algorithm-dependent. As a drawback of this approach, the selection of the best model is far from trivial since the scoring functions output by different servers are not comparable, and models need to be re-scored for evaluation with the same algorithms. As depicted in Supplementary Table S1, a first evaluation with QMEAN4 [50], which combines four statistical potential terms that range from 0 to 1, reveals that the model downloaded from the AlphaFold server is the most reliable and the second-best value of the degree of nativeness (i.e. Z-score), whereas the output by Swiss model is the second in reliability and the first in degree of nativeness, with the additional advantage that it is the only one that models the quaternary structure. The model by RaptorX also shows good scores, but worse than those by the AlphaFold model. The others are even worse. Hence, our analysis focuses on the AlphaFold and Swiss model.

Typical catalases are homotetrameric enzymes with 222 point group of symmetry, a feature output by the Swiss model server, every subunit contacting with the other three to yield the tetramer (Figure 8, left). The analysis of the interfaces at PDBePISA reveals that contrary to what might be expected, the surface between the adjacent monomers A and B or C and D is smaller than that formed by monomers A and C or B and D (Table 2). In terms of hydrogen bonds and salt bonds, the interface A/D (and its equivalent B/C) is more tightly bonded, whereas the interface A/C (or B/D) contributes to the stability of the quaternary structure with a similar number of hydrogen and salt bonds. These data suggest that the putative tetrameric arrangement results not only from the interfaces along the 2-fold axis but also from those between A and C (or B and D).

Our experimental data from pepper catalase point towards a dimeric rather than to a tetrameric arrangement and, to further analyze this discrepancy, a search for structures in the protein data bank (PDB) that share similar interfaces to that predicted by the Swiss model was carried out. The closest related interfaces are those from the prokaryote *Bacillus pomulis* with resorcinol (surface B/C or A/D) or catechol (surface B/D or A/C), which is a typical homotetrameric catalase enzyme [51], but with none from the PDB for the interface A/B (or CD), despite that the similarity threshold was lowered to 20%.

This result highlights the singularity of the interface A/B (or C/D) and it was anticipated since the ΔG P-value (Table 2) for the interface A/B (or C/D) suggested that it is less hydrophobic than expected, a fact that in crystallography is interpreted as a crystal packing interface rather than as a biological interface. Additionally, it has been reported that an unstable catalase isolated from patients with a Swiss-type acatalasemia rapidly dissociates into inactive dimers with reduced heme content [52], features shared by our recombinant enzyme.

Although its role is under discussion, different heme catalases are able to bind the reductant NADPH [53]. The fact that the Swiss model can be fitted into the NADPH-binding human catalase (PDB accession code

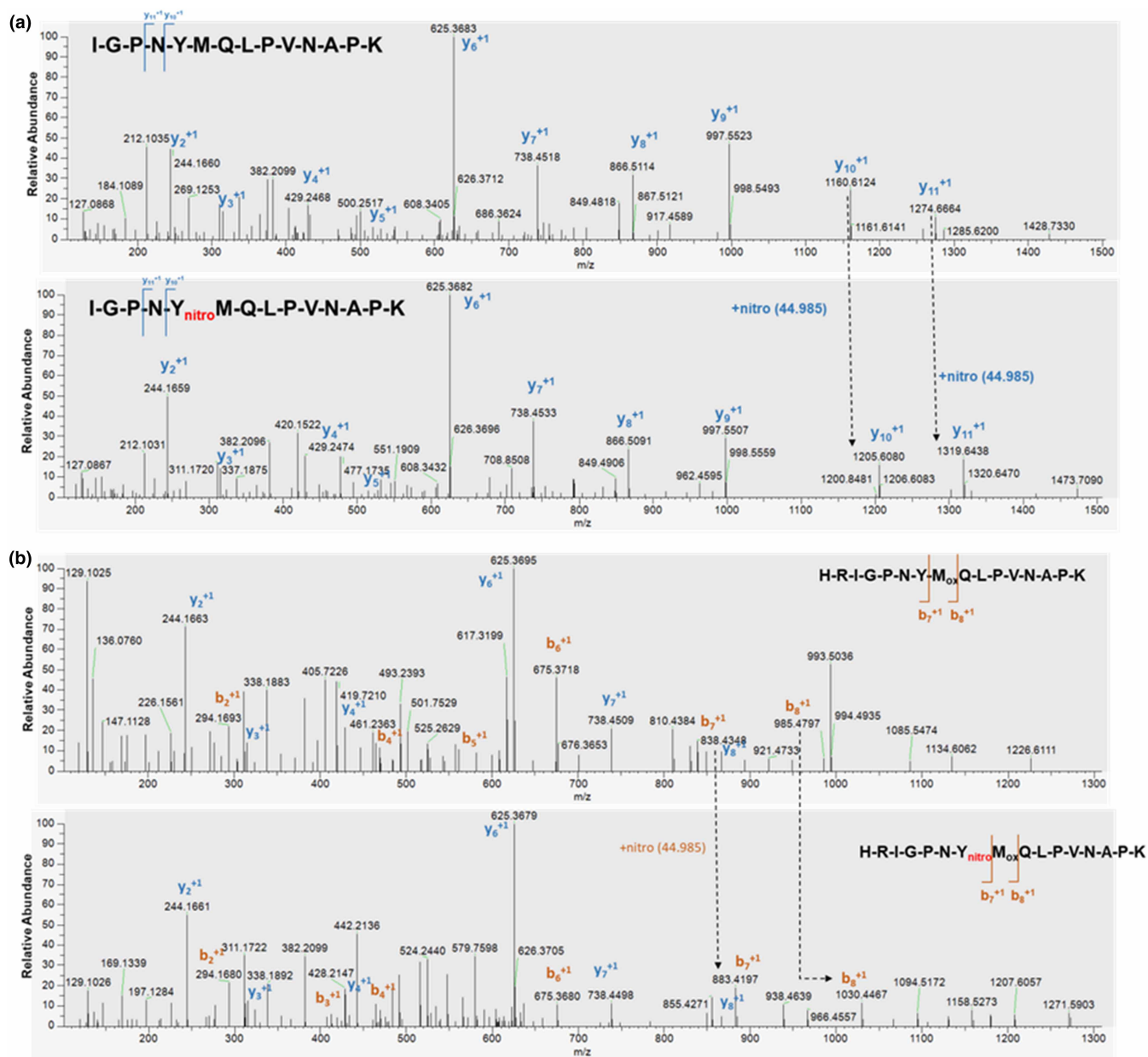


Figure 7. Identification by mass spectrometry of the tyrosine residues of the pepper catalase susceptible to being nitrated.

Mass spectrometry fragmentation spectra of the sweet pepper catalase corresponding to the unlabeled (upper panel) and labeled (Y-nitro, lower panel) version of peptides. (a) IGPNYMQLPVNAPK and (b) HRIGPNYMQLPVNAPK polypeptides show that both contain the nitrated Tyr348 and Tyr360 residues, respectively. The fragments corresponding to the main fragmentation series are denoted as “b” if the charge is retained on the N-terminus (red) and as “y” if the charge is maintained on the C-terminus (blue). The subscript in both series (b_n , y_n) indicates the number of amino acid residues in the considered fragment from either N-terminus or C-terminus. The superscript refers to the charge (+1) of the backbone fragmentation. Dotted arrows connecting both graphs in (a,b) indicate the increase of +44 985 Da corresponding to the modification Y/Ynitro.

1d_{gf}) with RMS 0.829 (427 atom pairs) encouraged us to study the preservation of the residues present in the NADPH sites. In the human enzyme, residues P151, V302, and W303, residues H194, F446, and V450, and residues R203, N213, and K237 are involved in the interactions with the nicotinamide, ribose, and phosphate motifs of the NADPH, respectively [54]. Additionally, S201 and H350 establish hydrogen bonds with NADPH. As depicted in Supplementary Figure S1, some of these residues are present in the molecule from *C. annuum*,

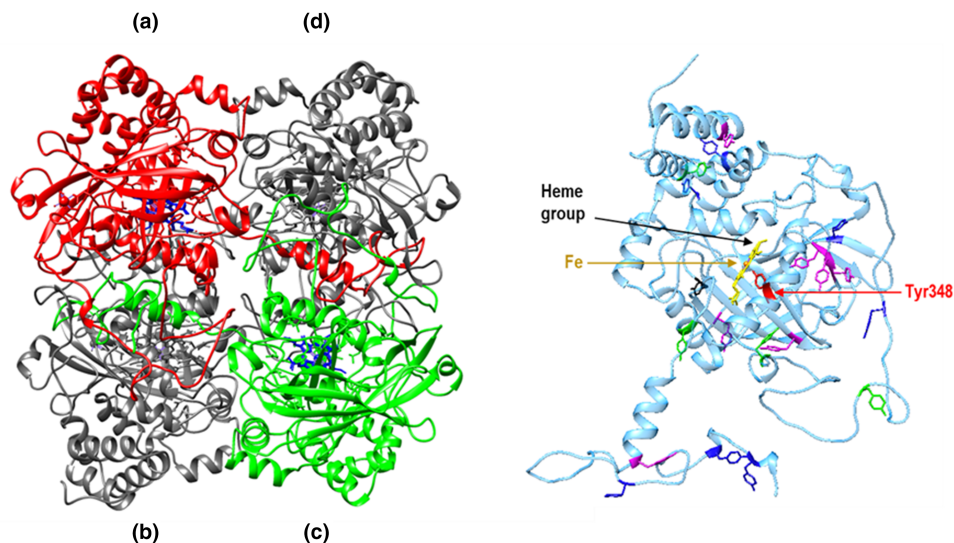
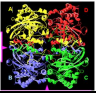

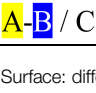


Figure 8. Left: Model output by Swiss model showing the putative tetrameric structure with subunits A and C colored in red and green, respectively (with cofactor in blue) to highlight the interactions among monomers. Right: Model downloaded from AlphaFold showing the Tyr residues colored in magenta when detected as nitrated, in blue when predicted as phosphorylated by both NetPhos3.1 and GPS_6.0 servers, and green when detected as nitrated and predicted as phosphorylated by both servers and in red Tyr348. In yellow color it is shown the heme group with the Fe atom in brown.

but it is significant the fact that only K237 is preserved among the residues that interact with the phosphate moiety, whereas neither H350 nor S201 are preserved. This result was not unexpected since, to the best of our knowledge, none of the plant catalases has been reported to bind NADPH.

Since the model downloaded from AlphaFold shows the best parameters of quality, it was used to study the different tyrosine residues in terms of pKa, solvent-accessible area (ASA), and tyrosine phosphorylation (Table 3). The primary structure of the catalase from *C. annuum* comprises 20 tyrosine residues distributed throughout the structure (Figure 9, right), and the *in vitro* treatment of the recombinant catalase with 3-morpholinomethylhydrazine (SIN-1), as a peroxynitrite donor, yielded the nitration of 12 tyrosine residues. However, the modulation of the enzyme by this extensive nitration seems unfeasible. In fact, residues Y256, Y360, Y392, and Y446 are also predicted as phosphorylated by both NetPhos 3.1 and GPS_6.0 servers. Residues with a low solvent accessible area (i.e. $<9 \text{ \AA}^2$) are Y190, Y199, Y210, Y435, Y446, and Y392 interfacial residues with limited accessibility. Considering that (i) tyrosine nitration occurs through a radical mechanism

Table 2. Analysis of the interfaces of the catalase from *Capsicum annuum* output by Swiss model and in parenthesis those from *Bacillus pumilis* that share the highest similarity.

Interface	# Residues	Surface (\AA^2)	ΔG (kcal/mol)	ΔG P-value	# H-bonds	#Salt bonds
 A-D / B-C	108/106 (109/107)	4068.8 (4239.2)	−42.7 (−31.6)	0.248 (0.092)	59 (63)	29 (34)
 A-C / B-D	102/101 (113/114)	38.996 (4324.5)	−46.5 (−38.1)	0.151 (0.058)	34 (47)	6 (2)
 A-B / C-D	57/60	2101.4	−11.0	0.764	36	8

Surface: difference in total accessible surface areas of isolated and interfacing structures divided by two. ΔG : indicates the solvation free energy gain upon formation of the interface, in kcal/M. ΔG P-value: measures the probability of getting a lower than observed ΔG , when the interface atoms are picked randomly from the protein surface. $P > 0.5$ means that the interface is less hydrophobic than it could be, therefore the interface is likely to be an artifact of crystal packing.

Table 3. Analysis of the tyrosine residues of the catalase from *Capsicum annuum*.

Residue	pKa	ASA (Å ²)	Phosphorylation	
			NetPhos3.1 (threshold >0.5)	GPS_6.0 (score/threshold >2.5)
Tyr6	10.12	143	Y	Y (EGFR)
Tyr12	10.25	143	Y	Y (Abl/EGFR/InsR)
Tyr26	10.21	223	Y	Y (Abl)
Tyr45	11.11	142		Y
Tyr127	13.40	26		
Tyr190	12.76	4	Y	Y
Tyr199	13.54	2		Y
Tyr210	12.58	0		
Tyr221	12.93	26	Y	Y
Tyr256	10.23	127	Y	Y (Abl/InsR)
Tyr264	10.21	115		Y
Tyr334	10.49	74		Y
Tyr335	11.91	36		
Tyr348	9.81	45		
Tyr360	11.57	16	Y	(Abl)
Tyr392	10.01	129	Y	Y (EGFR/Trk)
Tyr406	11.53	108	Y	Y (Abl)
Tyr435	12.20	7	Y	Y
Tyr446	14.35	5	Y	Y
Tyr470	11.64	31		Y (Trk)

Tyr nitrated by SIN-1 are shown in bold. The estimation of the pKa and accessible solvent area (ASA) was carried out from the model downloaded from AlphaFold and the prediction of the phosphorylation from the primary structure. Positive hits of Tyr phosphorylation are denoted by Y and the kinase, when identified, in parentheses.

[55–57], (ii) the nitration agent is NO₂ resulting from the reaction of peroxynitrite with carbon dioxide or a metal center [55], and (iii) the phenolate ion and not the phenol is straightforward oxidized to the phenoxy radicals [58], the ideal tyrosine residue should be acidic, accessible and close to the heme group. Y348 is the axial residue of the penta-co-ordinated heme group, with the lowest pKa value, with ASA of 45 Å² that best fulfills the above requirements. In fact, Y348 is equivalent to Y358 in the human catalase, which has been proposed to be part of a charge relay absolutely conserved that tunes the metal site [54]. A second candidate is Y360, which is equivalent to Y370 in the human enzyme and that was proposed as the tyrosine radical involved in the one-electron reduction in the porphyrin π -cation when NADPH is not available [54].

Discussion

Pepper fruit ripening is a complex process involving significant physiological and biochemical changes [4,6]. It is tightly regulated by hormonal and environmental cues, ensuring the successful maturation of the fruit. One of the most obvious changes is the conversion of chloroplasts to chromoplasts and the associated color change. Chloroplasts are responsible for photosynthesis, contributing to the fruit's growth and development. As the fruit matures and ripens, chlorophyll degrades, and chloroplasts transform into chromoplasts. This transformation involves the breakdown of thylakoid membranes and the accumulation of carotenoids, which are pigments responsible for the red, yellow, purple, or orange colors in ripe peppers. Carotenoids, such as β -carotene, violoxanthin, lutein, or capsorubin, are synthesized during this conversion process. Their increase results in the observable color change from green to red, yellow, purple, or orange, depending on the pepper variety [59–61]. Additionally, previous data indicate the ripening of pepper is associated with a very active metabolism of ROS and RNS since different enzymatic systems involved in the generation and scavenging of ROS/RNS as APX,

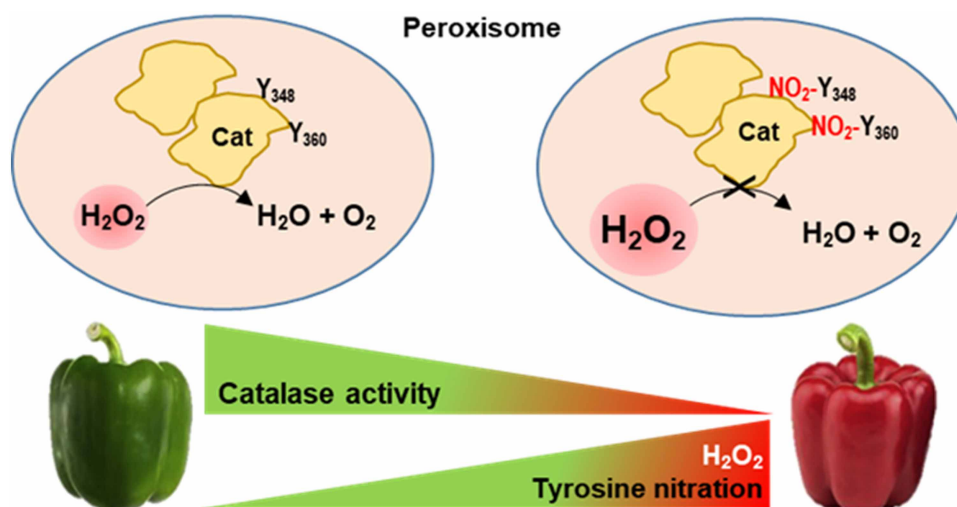


Figure 9. A proposed model summarizes that the activity of the pepper homodimer catalase (Cat) is down-regulated during fruit ripening.

This process is characterized by an increase of protein tyrosine nitration, where catalase is one of the main targets, especially in the tyrosine (Y) residues Y348 and Y360, which provokes the activity inhibition and an increase of the H_2O_2 content.

NADPH oxidase, superoxide dismutase, or S-nitrosogluthathione reductase, among others, suggesting that this process undertakes physiological nitro-oxidative stress [7,47,62,63]. Ascorbate, a key non-enzymatic antioxidant, plays multiple roles in pepper fruit development and ripening. During ripening, the concentration of ascorbate in the fruit increases [5]. Under a NO-enriched atmosphere, this increase is even more pronounced due to a simultaneous rise in the activity, protein levels, and gene expression of mitochondrial galactono-1,4-lactone dehydrogenase, the final enzyme in ascorbate biosynthesis [5]. Besides its role in antioxidant defense, ascorbate is also involved in cell wall metabolism, regulation of enzyme activities (such as APX and ascorbate oxidase), interaction with hormonal pathways, and contribution to color development. Furthermore, ascorbate ensures the healthy and orderly ripening of pepper fruits, leading to optimal quality and nutritional value. To get a deeper knowledge of the physiological and functional relevance of the antioxidant systems in the ripening process of pepper fruits, the present study focuses on catalase which is the main antioxidant enzyme present in peroxisomes [49]. The analysis has been accomplished at the transcriptomic, proteomic, and biochemical levels during maturation and under an enriched NO atmosphere. Furthermore, it identifies the Tyr residues target of nitration which triggers the down-regulation of the activity, and elucidates the quaternary structure of the enzyme in pepper fruits. Previous studies have provided the gene identification of pepper catalases and their expression analysis in different organs of hot pepper plants including roots, stems, flowers, and fruits [64,65]; however, to our knowledge there are no specific studies on the characterization and expression at the RNA and protein level of the three catalases during ripening in sweet pepper fruits and exposed to enriched NO environment.

The number of CAT genes identified and expressed in pepper fruits is similar to that reported for other species such as tobacco (*Nicotiana plumbaginifolia*) [66,67], maize (*Zea mays* L.) [68], pumpkin (*Cucurbita* Linn.) [27], *Arabidopsis thaliana* [30], and rice (*Oryza sativa* L.) [69,70]. However, there are species with different number of CAT genes. Thus, only one CAT gene has been reported in castor bean (*Ricinus communis* L.) [71], tomato (*Solanum lycopersicum*) [72], and sweet potato (*Ipomoea batatas* L.) [73]; 2 genes in barley (*Hordeum vulgare* L.) [74]; 4 in cucumber (*Cucumis sativus* L.) [19]; 6 in durum wheat (*Triticum turgidum* ssp. durum L.) [22]; 7 in cotton (*Gossypium hirsutum* L. and *Gossypium barbadense* L.) [21]; 10 in bread wheat (*Triticum aestivum* L.) [75]; 14 CAT genes in rapeseed (*Brassica napus* L.) [76]; and 16 in sugarcane (*Saccharum spontaneum*) [39]. However, the expression pattern of all these genes does not mean that they are expressed simultaneously, but rather it depends on the stage of development, the organ, and the environmental situation. On the other hand, the catalase isozymatic pattern does not have to coincide necessarily with the number of genes present in a particular plant species. For example, four catalase isozymes have been reported

in barley leaves under drought stress [77]; two in maize leaves [32]; and until a total of six catalase isozymes in *Arabidopsis* have been detected by non-denaturing gel electrophoresis in flower, four isozymes in leaves, bolt and silique, and two in roots [18,78]. In the case of pepper fruits, the analysis revealed the presence of a single isoenzyme by non-denaturing gel electrophoresis analysis. However, a previous study of pepper fruit by two-dimensional gel electrophoresis and MALDI-TOF allowed the distinction of several catalase subunits with MW ~57 kDa and pI between 6.6 and 7.3 [47].

Catalase is a key antioxidant enzyme present in peroxisomes and exerts an effective regulation of the content of H₂O₂ under physiological and stressful conditions [49,79]. In previous studies, we have analyzed catalase activity in pepper fruits and it was found that this enzyme is a main target of nitration [47,48]. The down-regulation of catalase activity during ripening was previously observed in different pepper fruit cultivars [47,80,81], but this decrease has been also found in other types of fruits like blackberry [82], tomato [83,84], guava [85], mango [86], mulberry [87] or olive [88]. Taken together, it seems that this is a characteristic of the ripening process which involves a lower H₂O₂ scavenging capacity and therefore this increase in H₂O₂ content [89] could contribute to the increase of lipid peroxidation found in ripe pepper fruit with a concomitant increase of lipoxygenase activity [6]. The relevance of the increase of H₂O₂ content in the ripening process is also supported by the activity of other H₂O₂ scavenging enzymes like APX whose total activity also decreased during pepper ripening [6], whereas the superoxide (O₂^{•−})-generating NADPH oxidase activity had an opposite behavior since it underwent an increase in activity during ripening [63,90]. Furthermore, there are data showing that exogenous H₂O₂ treatment promotes early fruit ripening such as it occurs in the Kyoho grape [91,92]. Sweet pepper fruit also shows an increase in the level of H₂O₂ at the onset of ripening when fruits start to accumulate carotenoids [89], which is in good agreement with the down-regulation of catalase activity which involves a lower scavenging capacity of H₂O₂.

From a structural point of view, except for small variations, the plant catalase consists of a tetramer made up of four identical subunits, whose native molecular mass ranges from 220–350 kDa [49,93]. However, there are exceptions to this. Thus, in cottonseeds, five catalase isozymes have been identified by isoelectric focusing being designed A and B the more acidic isozymes, and C to E the less acidic ones that were the consequence of the combination of two different subunits encoding from two distinct *catalase* genes that were temporarily synthesized according to the seedling development [25,94]. In *Arabidopsis*, which contains three *CAT* genes, McClung [78] hypothesized that considering that catalase could be constituted as heterotetramers, a total of 15 distinct isozymes could be formed according to the possible combinations of the different subunits encoded by the three *CAT* genes. However, the detection of fewer heterotetrameric catalase isozymes indicates that there must be some specificity in the interaction of the subunits. Additionally, it has been reported that active tetrameric catalase is usually phosphorylated by protein kinases to maintain H₂O₂ homeostasis [95,96]. Serine, threonine, or tyrosine are the residues to be phosphorylated, and in rice under salinity conditions, the salt tolerance receptor-like cytoplasmic kinase 1 (STRK1) phosphorylates rice CatC at Tyr210 increasing its activity [97]. On the other hand, very recently in rice peroxisomes, it has been shown that the tetramerization of catalase is also regulated by de-phosphorylation at Ser9 by a phosphatase of catalase 1 (PC1) which inhibits such tetramerization and consequently its activity [98]. Those two residues indicated above, Tyr210 and Ser9, involved in the phosphorylation/dephosphorylation, are both conserved in the three pepper catalase isozymes.

However, in the case of pepper fruit, a previous study by non-denaturing electrophoresis using the Hedrick and Smith method and gel filtration by FPLC showed that catalase behaves as a homodimer with a molecular mass in a native state between 125 and 135 kDa [48]. Likewise, the catalase modeling reported in this work supports that, in the case of pepper, catalase is homodimeric and corroborates the mentioned previous data obtained through chromatography and native electrophoresis [48], unlike what has been described in other plant and animal species. Thus, the dimeric arrangement of the recombinant pepper catalase could be due to that the interface between monomers A and B, and C and D is not present in the PDB, and the ΔG *P*-value does not support a biological interface (see Table 2). It should be also mentioned that although the model of the quaternary structure of the pepper catalase matches the NADPH-binding human catalase [99–101], including the NADPH site, and the same residues are preserved, most of those involved in the interaction with the phosphate moiety are not present and the enzyme is not expected to bind NADPH, which is a common feature of all plant catalases. Additionally, among the tyrosine residues detected as nitrated by MS analysis, features of the Tyr348 make it especially reactive and the Tyr360 is equivalent to Tyr370 in the human enzyme [54], which has been proposed as the tyrosyl radical involved in the one-electron reduction in the porphyrin π -cation in the absence of NADPH.

On the other hand, there is no direct correlation between gene and protein expression of the corresponding catalase isozymes encoded by three *CAT* genes identified in the present study. Likewise, the activity of catalase does not follow the same pattern, so regulation must be at different levels where protein PTMs must be key factors. Previously, it has been shown that catalase could be a target of NO-derived PTMs such as S-nitrosation and that tyrosine nitration can inhibit catalase activity [48,102,103] as well as a hydrogen sulfide (H_2S)-derived PTM persulfidation [104,105], all of them causing a down-regulation in activity. In the case of pepper catalase, we reported that the activity is negatively modulated by S-nitrosation and nitration [47,48]. We also identified by 2D electrophoresis in combination with antibodies against NO_2 -Tyr that pepper catalase during ripening is predominantly nitrated, which would be in good agreement with the observed activity data. However, to the best of our knowledge, thus far there were no data on which Tyr residue(s) was(were) the target(s) of nitration in any plant catalase system. Therefore, the MS analysis of the recombinant Cat3 reported here indicates that Tyr348 and Tyr360 are nitrated and, together with the modeling prediction, it shows how these nitrated residues support the inhibitory effect exerted by nitration, residues that interestingly are conserved in the three capsicum catalase isoenzymes (see Supplementary Figure S3).

In summary, the presented data provide new insights into the function and regulation of pepper catalase by NO and novel structural analysis which confirms the homodimeric conformation of this peroxisomal enzyme. Furthermore, to the best of our knowledge, it is the first identification of the Tyr residues from the pepper enzyme susceptible to being nitrated, thus supporting the inhibition of catalase activity during the pepper ripening and justifying the increase of H_2O_2 content necessary for this process, such as it has been observed in other fruits. Figure 9 provides a working model that summarizes these new elements described in this study indicating that the tyrosine nitration of Y348 and Y360 triggers the catalase inhibition.

Materials and methods

Plant material and NO gas treatment

The selection of California-sweet pepper (*C. annuum* L., cv. Melchor) fruits and their NO treatments were done according to González-Gordo et al. [6]. Concisely, pepper fruits were collected from plants grown in plastic-covered greenhouses (Syngenta Seeds, Ltd., El Ejido, Almería, Spain). Fruits without any apparent injuries at three developmental stages were marked as green immature (G), breaking point (BP1 and BP2), and red ripe (R). From the BP1 stage two additional groups of fruits were prepared, one was exposed to NO gas treatment (5 ppm NO for 1 h) as described earlier [106] and was designed BP2 + NO, and the other group without NO treatment used as an internal control named BP2 – NO. These fruits were maintained for three days at room temperature before they were processed. Supplementary Figure S1 displays the experimental design followed in this study with the characteristic phenotypes of pepper fruits at different ripening stages and exposed to NO treatment [7].

Library preparation and RNA-sequencing

The preparation of the pepper fruit libraries was done using an optimized Illumina protocol and they were sequenced on an Illumina NextSeq550 platform using 2×75 bp paired-end reads such as was reported previously [6]. The obtained reads were pre-managed to eliminate low-quality sequences and then, it was accomplished the *de novo* transcriptome assembly. Bowtie2 was used to realign the reads and Samtools to quantify known transcripts. Differential expression analyses were carried out using DEgenes-Hunter [107]. Sequence Read Archive data are available at the following link <https://www.ncbi.nlm.nih.gov/sra/PRJNA668052>.

Pepper proteome by iTRAQ® (Isobaric tags for relative and absolute quantitation)

Proteomic analysis was accomplished as described recently [8]. After reduction and alkylation, protein samples were mixed with trypsin at a final trypsin:protein ratio of 1:10 and digested overnight at 37°C. Tryptic peptides were dried by vacuum centrifugation, reconstituted in labeling buffer (70% ethanol/25 mM triethylammonium bicarbonate, TEAB), and labeled with iTRAQ reagents, according to the manufacturer's protocol (ABSciex, Framingham, MA, U.S.A.). Protein identification and quantification were performed by LC–MS/MS analysis using a nanoLC Ultra 1D plus/Triple TOF 5600 analyzer (ABSciex, Framingham, MA, U.S.A.).

Preparation of crude extracts and catalase activity assays

Frozen samples of sweet pepper fruits at the different ripening stages and after NO treatment were powdered under liquid nitrogen using an IKA® A11Basic analytical mill (IKA®, Staufen, Germany), and then extracted in 100 mM Tris–HCl buffer, pH 8.0, containing 0.1% (v/v) Triton X-100, 1 mM ethylenediaminetetraacetic acid, 10% (v/v) glycerol in a final 1:1 (w:v) plant material:buffer ratio. Protein content in the fruit samples was estimated using a Bio-Rad protein assay solution (Bio-Rad Laboratories, Hercules, CA, U.S.A.), with bovine serum albumin as standard.

The spectrophotometry assay of catalase activity was determined by following the breakdown of H₂O₂ at 240 nm as described by Aebi [108].

In-gel catalase activity was done in non-denaturing 6% polyacrylamide gels. The activity was detected according to the method described by Clare et al. [109]. Shortly, after the electrophoresis the gels were submerged for 45 min in 50 mM phosphate buffer, pH 7.0, containing 50 µg/ml horseradish peroxidase (Type II, 250 units/mg, Merck KGaA, Darmstadt, Germany). Then, 0.5 mM H₂O₂ was added to the solution and incubated for 10 min under dark conditions. Afterward, the gels were stained with a solution of phosphate buffer, pH 7.0, containing 0.5 mg/ml 3,3-diaminobenzidine until colorless bands appeared over a brown background. Band intensity was quantified with the aid of Image J 1.45 software.

Recombinant *C. annuum* catalase (CAT), protein modeling, and *in silico* analyses

The gene encoding CaCAT3 (Q9M5L6 Protein ID: NP_001311603.1, see Table 1) with an N-terminal 10xHis tag was codon-optimized for its heterologous expression in *Pichia pastoris* systems according to the standard protocol developed by Genosphere Biotechnologies (France). Recombinant CaCat3 from the yeast extract was purified by immobilized metal affinity chromatography with an expected size of 58.035 kDa and a purity of higher than 80%. The presence of the His tag was detected by immunoblot using a mouse anti-6xHis monoclonal antibody (dilution 1:2000).

The 3D structure of the catalase from pepper was modeled by submitting the sequence deposited at UniParc database with the accession code UPI0007BFA371 to IntFold [110], M4T [111], Phyre2 [112], RaptorX [113] and Swiss model [114]. The output models, including that deposited at the AlphaFold database [115], were inspected with UCSF Chimera [116] and further evaluated at the Structural Analysis and Verification Server (SAVES v6.0) in terms of stereochemical quality (Procheck) [117], three-dimensional profiles (Verify3D) [118] and nonbonded atomic interactions (Errat) [119] and the scoring function Qmean4 [50].

The prediction of the tyrosine phosphorylation was carried out on the primary sequence of the protein (UniParc UPI0007BFA371) at the NetPhos3.1 [120] server and GPS_6.0 server [121]. Positive hits were those with scores higher than 0.5 (NetPhos3.1) and a score/cutoff ratio higher than 2.5 (GPS_6.0). The accessible solvent area (ASA) was computed with DSSP [122] and the pKa was predicted with PropKa v3.2 [123] as part of the APBS-PDB2PQR software suite [124].

The study of the interfaces among the subunits comprising the quaternary structure and the search for similar structures in the PDB were carried out at PDBePISA [125]. As described in the documentation of the algorithm, the surface is estimated as the difference in total accessible surface areas of isolated and interfacing structures divided by 2. ΔG is calculated as the difference in total solvation energies of isolated and interfacing structures. It does not include the effect of satisfied hydrogen bonds and salt bridges across the interface. ΔG *P*-value is a measure of the probability of obtaining a lower than the output ΔG when the interface atoms are picked randomly from the protein surface. For the search of similar surfaces in PDB, only those structures with the monomers forming the interface that shares 70% of similarity (i.e. percentage of structure alignment) were considered, regardless of the multimeric assembly or whether other surfaces might be present.

In vitro treatment with peroxynitrite (ONOO[−]), SDS–PAGE and immunoblot analyses

For *in vitro* assays, recombinant CaCAT3 was incubated at 37°C for 2 h in darkness with increasing concentrations (0, 0.5, 1.0, 2.0, and 5.0 mM) of 3-morpholiniosydnonimine (SIN-1), a peroxynitrite donor [9].

SDS–PAGE was carried out in 4–20% precast polyacrylamide gel using a Mini-Protean electrophoresis cell (Bio-Rad, Hercules, CA, U.S.A.). For immunoblot analyses, the recombinant catalase treated with peroxynitrite was transferred onto 0.22 µm PVDF membranes using a Trans-Blot® Turbo™ Transfer Starter System

(Bio-Rad, Hercules, CA, U.S.A.). After transfer, the membranes were used for cross-reactivity assays with either a rabbit polyclonal antibody against nitro-tyrosine (Sigma #N 0409) diluted 1:2000. For immunodetection, an affinity-purified goat anti-rabbit IgG horseradish peroxidase conjugate (Bio-Rad Laboratories) and an enhanced chemiluminescence kit (Clarity™ Western ECL Substrate, Bio-Rad) were used. Chemiluminescence was analyzed using a Molecular Imager® Gel Doc™ XR documentation system.

Identification of nitrated tyrosine in recombinant catalase by liquid chromatography-electrospray ionization tandem mass spectrometry (LC-ESI-MS/MS)

Aliquots of purified catalase untreated (control) and treated with peroxyxynitrite (nitrating agent) were individually digested with trypsin using a standard protocol previously described [12]. Briefly, 10 µg of precipitated recombinant protein were resuspended and denatured in 10 µl of 7 M urea, 2 M thiourea, 100 mM TEAB, reduced with 5 mM Tris 2-carboxyethyl phosphine (TCEP; AB SCIEX, Foster City, CA, U.S.A.), pH 8.0, at 37°C for 60 min, and followed by the cysteine-blocking reagent chloroacetamide. Samples were diluted up to 50 µl with 25 mM TEAB to reduce the urea concentration. Sequence grade-modified trypsin (Pierce) was added to each sample (ratio 1:20 enzyme:sample), which was then incubated at 37°C overnight on a shaker. After digestion, samples were dried in a SpeedVac device (Thermo Scientific, Waltham, MA, U.S.A.). Before MS analysis, sample cleaning was performed using ZipTip C18 tips (Millipore). Each sample was subjected to one-dimensional-nano LC ESI-MS/MS (Liquid Chromatography Electrospray Ionization Tandem Mass Spectrometry) analysis using an Ultimate 3000 nano HPLC system (Thermo Fisher Scientific) coupled online to an Orbitrap Exploris 240 mass spectrometer (Thermo Fisher Scientific).

Catalase peptides were eluted onto a 15 cm × 75 µm Easy-spray PepMap C18 analytical column at 45°C and separated at a flow rate of 300 nl/min using a 40 min gradient ranging from 2% to 35% mobile phase B [mobile phase A: 0.1% formic acid (FA); mobile phase B: 80% acetonitrile (ACN) in 0.1% FA]. The loading solvent was 2% ACN in 0.1% FA, and the injection volume was 5 µl.

Data acquisition was performed using a data-dependent top-20 method, in full scan positive mode, scanning 375–1200 m/z. Survey scans were acquired at a resolution of 60 000 at 200 m/z, with a Normalized Automatic Gain Control (AGC) target (%) of 300 and a maximum injection time (IT) in AUTO mode. The top 20 most intense ions from each MS1 scan were selected and fragmented via higher-energy collisional dissociation (HCD). Resolution for HCD spectra was set to 45 000 at m/z 200, with an AGC target of 100 and a maximum ion IT in AUTO mode. Isolation of precursors was performed with a window of 0.7 m/z, exclusion duration (s) of 5 sec and the HCD collision energy was 30. Precursor ions with single, unassigned, or six and higher charge states from fragmentation selection were excluded.

Data Availability

All data relevant to this paper are included in the manuscript.

Competing Interests

The authors declare that there are no competing interests associated with the manuscript information

Funding

Our research is supported by a European Regional Development Fund co-financed grants from the Ministry of Science and Innovation (PID2019-103924GB-I00 and CPP2021-008703), Spain.

CRedit Author Contribution

Francisco J. Corpas: Conceptualization, Writing — original draft, Project administration. **Salvador González-Gordo:** Formal analysis, Investigation. **Javier López-Jaramillo:** Formal analysis, Investigation. **Marta Rodríguez-Ruiz:** Formal analysis, Investigation. **Jorge Taboada:** Software, Formal analysis. **José M. Palma:** Writing — review and editing.

Open Access

Open access for this article was enabled by the participation of Spanish National Research Council (CSIC) in an all-inclusive *Read & Publish* agreement with Portland Press and the Biochemical Society.

Acknowledgements

S.G.-G. acknowledges a ‘Formación de Personal Investigador’ contract (BES-2016-078368) from the Ministry of Science and Innovation, Spain. The provision of pepper fruits by Syngenta Seeds Ltd (El Ejido, Almería, Spain) is acknowledged, especially to Víctor J. Domínguez, Lidia Martín and Manuel Solís. The technical support of Dr. Alberto Paradela of the Proteomic Core Facility (CNB-CSIC, Madrid, Spain) is also acknowledged. The valuable technical assistance of Mrs. María J. Campos and Mr. Carmelo Ruiz-Torres is deeply acknowledged.

Abbreviations

ACN, acetonitrile; APX, ascorbate peroxidase; CRE, cis-regulatory element; FA, formic acid; HCD, higher-energy collisional dissociation; IT, injection time; MS, mass spectrometry; NO, nitric oxide; PDB, protein data bank; PTM, posttranslational modification; RNS, reactive nitrogen species.

References

- Baenas, N., Belović, M., Ilic, N., Moreno, D.A. and García-Viguera, C. (2019) Industrial use of pepper (*Capsicum annuum* L.) derived products: technological benefits and biological advantages. *Food Chem.* **274**, 872–885 <https://doi.org/10.1016/j.foodchem.2018.09.047>
- Qiu, Y., Li, Y., Wu, L., Wei, H., Fu, J., Chen, W. et al. (2023) Analysis of important volatile organic compounds and genes produced by aroma of pepper fruit by HS-SPME-GC/MS and RNA sequencing. *Plants (Basel)* **12**, 2246 <https://doi.org/10.3390/plants12122246>
- Guevara, L., Domínguez-Anaya, M.Á., Ortigosa, A., González-Gordo, S., Díaz, C., Vicente, F. et al. (2021) Identification of compounds with potential therapeutic uses from sweet pepper (*Capsicum annuum* L.) fruits and their modulation by nitric oxide (NO). *Int. J. Mol. Sci.* **22**, 4476 <https://doi.org/10.3390/ijms22094476>
- Palma, J.M., Sevilla, F., Jiménez, A., del Río, L.A., Corpas, F.J., Álvarez de Morales, P. et al. (2015) Physiology of pepper fruit and the metabolism of antioxidants: chloroplasts, mitochondria and peroxisomes. *Ann. Bot.* **116**, 627–636 <https://doi.org/10.1093/aob/mcv121>
- Rodríguez-Ruiz, M., Mateos, R.M., Codesido, V., Corpas, F.J. and Palma, J.M. (2017) Characterization of the galactono-1,4-lactone dehydrogenase from pepper fruits and its modulation in the ascorbate biosynthesis. Role of nitric oxide. *Redox Biol.* **12**, 171–181 <https://doi.org/10.1016/j.redox.2017.02.009>
- González-Gordo, S., Bautista, R., Claros, M.G., Cañas, A., Palma, J.M. and Corpas, F.J. (2019) Nitric oxide-dependent regulation of sweet pepper fruit ripening. *J. Exp. Bot.* **70**, 4557–4570 <https://doi.org/10.1093/jxb/erz136>
- González-Gordo, S., Rodríguez-Ruiz, M., López-Jaramillo, J., Muñoz-Vargas, M.A., Palma, J.M. and Corpas, F.J. (2022) Nitric oxide (NO) differentially modulates the ascorbate peroxidase (APX) isozymes of sweet pepper (*Capsicum annuum* L.) fruits. *Antioxidants (Basel)* **11**, 765 <https://doi.org/10.3390/antiox11040765>
- González-Gordo, S., Palma, J.M. and Corpas, F.J. (2022) Peroxisomal proteome mining of sweet pepper (*Capsicum annuum* L.) fruit ripening through whole isobaric tags for relative and absolute quantitation analysis. *Front. Plant Sci.* **13**, 893376 <https://doi.org/10.3389/fpls.2022.893376>
- González-Gordo, S., Muñoz-Vargas, M.A., Palma, J.M. and Corpas, F.J. (2023) Class III peroxidases (POD) in pepper (*Capsicum annuum* L.): genome-wide identification and regulation during nitric oxide (NO)-influenced fruit ripening. *Antioxidants (Basel)* **12**, 1013 <https://doi.org/10.3390/antiox12051013>
- González-Gordo, S., Palma, J.M. and Corpas, F.J. (2023) Small heat shock protein (sHSP) gene family from sweet pepper (*Capsicum annuum* L.) fruits: involvement in ripening and modulation by nitric oxide (NO). *Plants (Basel)* **12**, 389 <https://doi.org/10.3390/plants12020389>
- Muñoz-Vargas, M.A., González-Gordo, S., Cañas, A., López-Jaramillo, J., Palma, J.M. and Corpas, F.J. (2018) Endogenous hydrogen sulfide (H₂S) is up-regulated during sweet pepper (*Capsicum annuum* L.) fruit ripening. In vitro analysis shows that NADP-dependent isocitrate dehydrogenase (ICDH) activity is inhibited by H₂S and NO. *Nitric Oxide* **81**, 36–45 <https://doi.org/10.1016/j.niox.2018.10.002>
- Muñoz-Vargas, M.A., López-Jaramillo, J., González-Gordo, S., Paradela, A., Palma, J.M. and Corpas, F.J. (2023) H₂S-generating cytosolic L-cysteine desulfhydrase (LCD) and mitochondrial D-cysteine desulfhydrase (DCD) from sweet pepper (*Capsicum annuum* L.) are regulated during fruit ripening and by nitric oxide (NO). *Antioxid. Redox Signal.* **39**, 2–18 <https://doi.org/10.1089/ars.2022.0222>
- Muñoz-Vargas, M.A., González-Gordo, S., Taboada, J., Palma, J.M. and Corpas, F.J. (2023) In silico RNAseq and biochemical analyses of glucose-6-phosphate dehydrogenase (G6PDH) from sweet pepper fruits: involvement of nitric oxide (NO) in ripening and modulation. *Plants (Basel)* **12**, 3408 <https://doi.org/10.3390/plants12193408>
- Taboada, J., González-Gordo, S., Muñoz-Vargas, M.A., Palma, J.M. and Corpas, F.J. (2023) NADP-dependent malic enzyme genes in sweet pepper fruits: involvement in ripening and modulation by nitric oxide (NO). *Plants (Basel)* **12**, 2353 <https://doi.org/10.3390/plants12122353>
- Corpas, F.J., González-Gordo, S. and Palma, J.M. (2020) Plant peroxisomes: a factory of reactive species. *Front. Plant Sci.* **11**, 853 <https://doi.org/10.3389/fpls.2020.00853>
- Baudhuin, P., Beaufay, H. and De Duve, C. (1965) Combined biochemical and morphological study of particulate fractions from rat liver. Analysis of preparations enriched in lysosomes or in particles containing urate oxidase, D-amino acid oxidase, and catalase. *J. Cell Biol.* **26**, 219–243 <https://doi.org/10.1083/jcb.26.1.219>
- Leighton, F., Poole, B., Lazarow, P.B. and De Duve, C. (1969) The synthesis and turnover of rat liver peroxisomes. I. Fractionation of peroxisome proteins. *J. Cell Biol.* **41**, 521–535 <https://doi.org/10.1083/jcb.41.2.521>
- Frugoli, J.A., Zhong, H.H., Nuccio, M.L., McCourt, P., McPeck, M.A., Thomas, T.L. et al. (1996) Catalase is encoded by a multigene family in *Arabidopsis thaliana* (L.) Heynh. *Plant Physiol.* **112**, 327–336 <https://doi.org/10.1104/pp.112.1.327>
- Hu, L., Yang, Y., Jiang, L. and Liu, S. (2016) The catalase gene family in cucumber: genome-wide identification and organization. *Genet. Mol. Biol.* **39**, 408–415 <https://doi.org/10.1590/1678-4685-GMB-2015-0192>
- Alam, N.B. and Ghosh, A. (2018) Comprehensive analysis and transcript profiling of *Arabidopsis thaliana* and *Oryza sativa* catalase gene family suggests their specific roles in development and stress responses. *Plant Physiol. Biochem.* **123**, 54–64 <https://doi.org/10.1016/j.plaphy.2017.11.018>

- 21 Wang, W., Cheng, Y., Chen, D., Liu, D., Hu, M., Dong, J. et al. (2019) The catalase gene family in cotton: genome-wide characterization and bioinformatics analysis. *Cells* **8**, 86 <https://doi.org/10.3390/cells8020086>
- 22 Ghorbel, M., Zribi, I., Besbes, M., Bouali, N. and Brini, F. (2023) Catalase gene family in durum wheat: genome-wide analysis and expression profiling in response to multiple abiotic stress conditions. *Plants (Basel)* **12**, 2720 <https://doi.org/10.3390/plants12142720>
- 23 Yamaguchi, J. and Nishimura, M. (1984) Purification of glyoxysomal catalase and immunochemical comparison of glyoxysomal and leaf peroxisomal catalase in germinating pumpkin cotyledons. *Plant Physiol.* **74**, 261–267 <https://doi.org/10.1104/pp.74.2.261>
- 24 Kunce, C.M. and Trelease, R.N. (1986) Heterogeneity of catalase in maturing and germinated cotton seeds. *Plant Physiol.* **81**, 1134–1139 <https://doi.org/10.1104/pp.81.4.1134>
- 25 Ni, W., Trelease, R.N. and Eising, R. (1990) Two temporally synthesized charge subunits interact to form the five isoforms of cottonseed (*Gossypium hirsutum*) catalase. *Biochem. J.* **269**, 233–238 <https://doi.org/10.1042/bj2690233>
- 26 Mullen, R.T. and Gifford, D.J. (1993) Purification and characterization of catalase from loblolly pine (*Pinus taeda* L.) megagametophytes. *Plant Physiol.* **103**, 477–483 <https://doi.org/10.1104/pp.103.2.477>
- 27 Esaka, M., Yamada, N., Kitabayashi, M., Setoguchi, Y., Tsugeki, R., Kondo, M. et al. (1997) cDNA cloning and differential gene expression of three catalases in pumpkin. *Plant Mol. Biol.* **33**, 141–155 <https://doi.org/10.1023/a:1005742916292>
- 28 Corpas, F.J., Palma, J.M., Sandalio, L.M., López-Huertas, E., Romero-Puertas, M.C., Barroso, J.B. et al. (1999) Purification of catalase from pea leaf peroxisomes: identification of five different isoforms. *Free Radic. Res.* **31**, S235–S241 <https://doi.org/10.1080/10715769900301561>
- 29 Matsumura, T., Tabayashi, N., Kamagata, Y., Souma, C. and Saruyama, H. (2002) Wheat catalase expressed in transgenic rice can improve tolerance against low temperature stress. *Physiol. Plant.* **116**, 317–327 <https://doi.org/10.1034/j.1399-3054.2002.1160306.x>
- 30 Du, Y.-Y., Wang, P.-C., Chen, J. and Song, C.-P. (2008) Comprehensive functional analysis of the catalase gene family in *Arabidopsis thaliana*. *J. Integr. Plant Biol.* **50**, 1318–1326 <https://doi.org/10.1111/j.1744-7909.2008.00741.x>
- 31 Mhamdi, A., Queval, G., Chaouch, S., Vanderauwera, S., Van Breusegem, F. and Noctor, G. (2010) Catalase function in plants: a focus on Arabidopsis mutants as stress-mimic models. *J. Exp. Bot.* **61**, 4197–4220 <https://doi.org/10.1093/jxb/erq282>
- 32 Horváth, E., Janda, T., Szalai, G. and Páldi, E. (2002) In vitro salicylic acid inhibition of catalase activity in maize: differences between the isozymes and a possible role in the induction of chilling tolerance. *Plant Sci.* **163**, 1129–1135 [https://doi.org/10.1016/S0168-9452\(02\)00324-2](https://doi.org/10.1016/S0168-9452(02)00324-2)
- 33 Valderama, R., Corpas, F.J., Carreras, A., Gómez-Rodríguez, M.V., Chaki, M., Pedrajas, J.R. et al. (2006) The dehydrogenase-mediated recycling of NADPH is a key antioxidant system against salt-induced oxidative stress in olive plants. *Plant Cell Environ.* **29**, 1449–1459 <https://doi.org/10.1111/j.1365-3040.2006.01530.x>
- 34 Sofo, A., Scopa, A., Nuzzaci, M. and Vitti, A. (2015) Ascorbate peroxidase and catalase activities and their genetic regulation in plants subjected to drought and salinity stresses. *Int. J. Mol. Sci.* **16**, 13561–13578 <https://doi.org/10.3390/ijms160613561>
- 35 Sousa, R.H.V., Carvalho, F.E.L., Ribeiro, C.W., Passaia, G., Cunha, J.R., Lima-Melo, Y. et al. (2015) Peroxisomal APX knockdown triggers antioxidant mechanisms favourable for coping with high photorespiratory H₂O₂ induced by CAT deficiency in rice. *Plant Cell Environ.* **38**, 499–513 <https://doi.org/10.1111/pce.12409>
- 36 Sousa, R.H.V., Carvalho, F.E.L., Lima-Melo, Y., Alencar, V.T.C.B., Daloso, D.M., Margis-Pinheiro, M. et al. (2019) Impairment of peroxisomal APX and CAT activities increases protection of photosynthesis under oxidative stress. *J. Exp. Bot.* **70**, 627–639 <https://doi.org/10.1093/jxb/ery354>
- 37 Houmani, H., Debez, A., de Freitas-Silva, L., Abdely, C., Palma, J.M. and Corpas, F.J. (2022) Potassium (K⁺) starvation-induced oxidative stress triggers a general boost of antioxidant and NADPH-generating systems in the halophyte *Cakile maritima*. *Antioxidants (Basel)* **11**, 401 <https://doi.org/10.3390/antiox11020401>
- 38 Mukarram, M., Khan, M.M.A., Kurjak, D. and Corpas, F.J. (2023) Chitosan oligomers (COS) trigger a coordinated biochemical response of lemongrass (*Cymbopogon flexuosus*) plants to palliate salinity-induced oxidative stress. *Sci. Rep.* **13**, 8636 <https://doi.org/10.1038/s41598-023-35931-w>
- 39 Wu, Q., Chen, Y., Zou, W., Pan, Y.-B., Lin, P., Xu, L. et al. (2023) Genome-wide characterization of sugarcane catalase gene family identifies a ScCAT1 gene associated disease resistance. *Int. J. Biol. Macromol.* **232**, 123398 <https://doi.org/10.1016/j.ijbiomac.2023.123398>
- 40 Kolbert, Z., Barroso, J.B., Brouquisse, R., Corpas, F.J., Gupta, K.J., Lindermayr, C. et al. (2019) A forty year journey: the generation and roles of NO in plants. *Nitric Oxide* **93**, 53–70 <https://doi.org/10.1016/j.niox.2019.09.006>
- 41 Corpas, F.J., González-Gordo, S. and Palma, J.M. (2022) NO source in higher plants: present and future of an unresolved question. *Trends Plant Sci.* **27**, 116–119 <https://doi.org/10.1016/j.tplants.2021.11.016>
- 42 Gupta, K.J., Kolbert, Z., Durner, J., Lindermayr, C., Corpas, F.J., Brouquisse, R. et al. (2020) Regulating the regulator: nitric oxide control of post-translational modifications. *New Phytol.* **227**, 1319–1325 <https://doi.org/10.1111/nph.16622>
- 43 Mishra, V., Singh, P., Tripathi, D.K., Corpas, F.J. and Singh, V.P. (2021) Nitric oxide and hydrogen sulfide: an indispensable combination for plant functioning. *Trends Plant Sci.* **26**, 1270–1285 <https://doi.org/10.1016/j.tplants.2021.07.016>
- 44 Yang, H., Wu, F. and Cheng, J. (2011) Reduced chilling injury in cucumber by nitric oxide and the antioxidant response. *Food Chem.* **127**, 1237–1242 <https://doi.org/10.1016/j.foodchem.2011.02.011>
- 45 Ren, Y., Xue, Y., Tian, D., Zhang, L., Xiao, G. and He, J. (2020) Improvement of postharvest anthracnose resistance in mango fruit by nitric oxide and the possible mechanisms involved. *J. Agric. Food Chem.* **68**, 15460–15467 <https://doi.org/10.1021/acs.jafc.0c04270>
- 46 Fan, S., Li, Q., Feng, S., Lei, Q., Abbas, F., Yao, Y. et al. (2022) Melatonin maintains fruit quality and reduces anthracnose in postharvest papaya via enhancement of antioxidants and inhibition of pathogen development. *Antioxidants (Basel)* **11**, 804 <https://doi.org/10.3390/antiox11050804>
- 47 Chaki, M., Álvarez de Morales, P., Ruiz, C., Begara-Morales, J.C., Barroso, J.B., Corpas, F.J. et al. (2015) Ripening of pepper (*Capsicum annuum*) fruit is characterized by an enhancement of protein tyrosine nitration. *Ann. Bot.* **116**, 637–647 <https://doi.org/10.1093/aob/mcv016>
- 48 Rodríguez-Ruiz, M., González-Gordo, S., Cañas, A., Campos, M.J., Paradela, A., Corpas, F.J. et al. (2019) Sweet pepper (*Capsicum annuum* L.) fruits contain an atypical peroxisomal catalase that is modulated by reactive oxygen and nitrogen species. *Antioxidants (Basel)* **8**, 374 <https://doi.org/10.3390/antiox8090374>
- 49 Palma, J.M., Mateos, R.M., López-Jaramillo, J., Rodríguez-Ruiz, M., González-Gordo, S., Lechuga-Sancho, A.M. et al. (2020) Plant catalases as NO and H₂S targets. *Redox Biol.* **34**, 101525 <https://doi.org/10.1016/j.redox.2020.101525>
- 50 Benkert, P., Tosatto, S.C.E. and Schomburg, D. (2008) QMEAN: a comprehensive scoring function for model quality assessment. *Proteins* **71**, 261–277 <https://doi.org/10.1002/prot.21715>

- 51 Loewen, P.C., Villanueva, J., Switala, J., Donald, L.J. and Ivancich, A. (2015) Unprecedented access of phenolic substrates to the heme active site of a catalase: substrate binding and peroxidase-like reactivity of *Bacillus pumilus* catalase monitored by X-ray crystallography and EPR spectroscopy. *Proteins* **83**, 853–866 <https://doi.org/10.1002/prot.24777>
- 52 Aebi, H. (1974) Catalase. In *Methods of Enzymatic Analysis*, 2nd edn (Bergmeyer, H.U., ed.), vol. **2**, pp. 673–684, Academic Press, Cambridge, MA
- 53 Zamocky, M., Furtmüller, P.G. and Obinger, C. (2008) Evolution of catalases from bacteria to humans. *Antioxid. Redox Signal.* **10**, 1527–1548 <https://doi.org/10.1089/ars.2008.2046>
- 54 Putnam, C.D., Arvai, A.S., Bourne, Y. and Tainer, J.A. (2000) Active and inhibited human catalase structures: ligand and NADPH binding and catalytic mechanism. *J. Mol. Biol.* **296**, 295–309 <https://doi.org/10.1006/jmbi.1999.3458>
- 55 Alvarez, B. and Radi, R. (2003) Peroxynitrite reactivity with amino acids and proteins. *Amino Acids* **25**, 295–311 <https://doi.org/10.1007/s00726-003-0018-8>
- 56 Radi, R. (2018) Oxygen radicals, nitric oxide, and peroxynitrite: redox pathways in molecular medicine. *Proc. Natl Acad. Sci. U.S.A.* **115**, 5839–5848 <https://doi.org/10.1073/pnas.1804932115>
- 57 Campolo, N., Issoglio, F.M., Estrin, D.A., Bartesaghi, S. and Radi, R. (2020) 3-Nitrotyrosine and related derivatives in proteins: precursors, radical intermediates and impact in function. *Essays Biochem.* **64**, 111–133 <https://doi.org/10.1042/EBC20190052>
- 58 Uppu, R.M., Lemerrier, J.N., Squadrito, G.L., Zhang, H., Bolzan, R.M. and Pryor, W.A. (1998) Nitrosation by peroxynitrite: use of phenol as a probe. *Arch. Biochem. Biophys.* **358**, 1–16 <https://doi.org/10.1006/abbi.1998.0825>
- 59 Filyushin, M.A., Dzhos, E.A., Shchennikova, A.V. et al. (2020) Dependence of pepper fruit colour on basic pigments ratio and expression pattern of carotenoid and anthocyanin biosynthesis genes. *Russ. J. Plant Physiol.* **67**, 1054–1062 <https://doi.org/10.1134/S1021443720050040>
- 60 Jang, S., Kim, G.W., Han, K., Kim, Y.M., Jo, J., Lee, S.Y. et al. (2022) Investigation of genetic factors regulating chlorophyll and carotenoid biosynthesis in red pepper fruit. *Front. Plant Sci.* **13**, 922963 <https://doi.org/10.3389/fpls.2022.922963>
- 61 Gómez-García, M.R. and Ochoa-Alejo, N. (2023) Biochemistry and molecular biology of carotenoid biosynthesis in chili peppers (*Capsicum* spp.). *Int. J. Mol. Sci.* **14**, 19025–19053 <https://doi.org/10.3390/ijms140919025>
- 62 Corpas, F.J., Freschi, L., Rodríguez-Ruiz, M., Miotto, P.T., González-Gordo, S. and Palma, J.M. (2018) Nitro-oxidative metabolism during fruit ripening. *J. Exp. Bot.* **69**, 3449–3463 <https://doi.org/10.1093/jxb/erx453>
- 63 González-Gordo, S., Rodríguez-Ruiz, M., Palma, J.M. and Corpas, F.J. (2020) Superoxide radical metabolism in sweet pepper (*Capsicum annuum* L.) fruits is regulated by ripening and by a NO-enriched environment. *Front. Plant Sci.* **11**, 485 <https://doi.org/10.3389/fpls.2020.00485>
- 64 Kwon, S.I. and An, C.S. (2001) Molecular cloning, characterization and expression analysis of a catalase cDNA from hot pepper (*Capsicum annuum* L.). *Plant Sci.* **160**, 961–969 [https://doi.org/10.1016/S0168-9452\(01\)00332-6](https://doi.org/10.1016/S0168-9452(01)00332-6)
- 65 Lee, S.H. and An, C.S. (2005) Differential expression of three catalase genes in hot pepper (*Capsicum annuum* L.). *Mol. Cells* **20**, 247–255 [https://doi.org/10.1016/S1016-8478\(23\)13224-9](https://doi.org/10.1016/S1016-8478(23)13224-9)
- 66 Willekens, H., Villarroel, R., Van Montagu, M., Inzé, D. and Van Camp, W. (1994) Molecular identification of catalases from *Nicotiana plumbaginifolia* (L.). *FEBS Lett.* **352**, 79–83 [https://doi.org/10.1016/0014-5793\(94\)00923-6](https://doi.org/10.1016/0014-5793(94)00923-6)
- 67 Willekens, H., Inzé, D., Van Montagu, M. and van Camp, W. (1995) Catalases in plants. *Mol. Breeding* **1**, 207–228 <https://doi.org/10.1007/BF02277422>
- 68 Guan, L. and Scandalios, J.G. (1995) Developmentally related responses of maize catalase genes to salicylic acid. *Proc. Natl Acad. Sci. U.S.A.* **92**, 5930–5934 <https://doi.org/10.1073/pnas.92.13.5930>
- 69 Joo, J., Lee, Y.H. and Song, S.I. (2014) Rice CatA, CatB, and CatC are involved in environmental stress response, root growth, and photorespiration, respectively. *J. Plant Biol.* **57**, 375–382 <https://doi.org/10.1007/s12374-014-0383-8>
- 70 Jiang, W., Ye, Q., Wu, Z., Zhang, Q., Wang, L., Liu, J. et al. (2023) Analysis of CAT gene family and functional identification of OsCAT3 in rice. *Genes (Basel)* **14**, 138 <https://doi.org/10.3390/genes14010138>
- 71 González, E. (1991) The C-terminal domain of plant catalases. Implications for a glyoxysomal targeting sequence. *Eur. J. Biochem.* **199**, 211–215 <https://doi.org/10.1111/j.1432-1033.1991.tb16111.x>
- 72 Drory, A. and Woodson, W.R. (1992) Molecular cloning and nucleotide sequence of a cDNA encoding catalase from tomato. *Plant Physiol.* **100**, 1605–1606 <https://doi.org/10.1104/pp.100.3.1605>
- 73 Chen, H.-J., Wu, S.-D., Huang, G.-J., Shen, C.-Y., Afiyanti, M., Li, W.-J. et al. (2012) Expression of a cloned sweet potato catalase SPCAT1 alleviates ethephon-mediated leaf senescence and H₂O₂ elevation. *J. Plant Physiol.* **169**, 86–97 <https://doi.org/10.1016/j.jplph.2011.08.002>
- 74 Skadsen, R.W., Schulze-Lefert, P. and Herbst, J.M. (1995) Molecular cloning, characterization and expression analysis of two catalase isozyme genes in barley. *Plant Mol. Biol.* **29**, 1005–1014 <https://doi.org/10.1007/BF00014973>
- 75 Zhang, Y., Zheng, L., Yun, L., Ji, L., Li, G., Ji, M. et al. (2022) Catalase (CAT) gene family in wheat (*Triticum aestivum* L.): evolution, expression pattern and function analysis. *Int. J. Mol. Sci.* **23**, 542 <https://doi.org/10.3390/ijms23010542>
- 76 Raza, A., Su, W., Gao, A., Mehmood, S.S., Hussain, M.A., Nie, W. et al. (2021) Catalase (CAT) gene family in rapeseed (*Brassica napus* L.): genome-wide analysis, identification, and expression pattern in response to multiple hormones and abiotic stress conditions. *Int. J. Mol. Sci.* **22**, 4281 <https://doi.org/10.3390/ijms22084281>
- 77 Rohman, M.M., Alam, S.S., Akhi, A.H., Begum, F. and Amiruzzaman, M. (2020) Response of catalase to drought in barley (*Hordeum vulgare* L.) seedlings and its purification. *Afr. J. Biotechnol.* **19**, 478–486 <https://doi.org/10.5897/AJB2020.17169>
- 78 McClung, C.R. (1997) Regulation of catalases in Arabidopsis. *Free Radic. Biol. Med.* **23**, 489–496 [https://doi.org/10.1016/S0891-5849\(97\)00109-3](https://doi.org/10.1016/S0891-5849(97)00109-3)
- 79 Yang, Z., Mhamdi, A. and Noctor, G. (2019) Analysis of catalase mutants underscores the essential role of CATALASE2 for plant growth and day length-dependent oxidative signalling. *Plant Cell Environ.* **42**, 688–700 <https://doi.org/10.1111/pce.13453>
- 80 Jiménez, A., Romojaro, F., Gómez, J.M., Llanos, M.R. and Sevilla, F. (2003) Antioxidant systems and their relationship with the response of pepper fruits to storage at 20°C. *J. Agric. Food Chem.* **51**, 6293–6299 <https://doi.org/10.1021/jf030052i>
- 81 Mateos, R.M., Jiménez, A., Román, P., Romojaro, F., Bacarizo, S., Leterrier, M. et al. (2013) Antioxidant systems from Pepper (*Capsicum annuum* L.): involvement in the response to temperature changes in ripe fruits. *Int. J. Mol. Sci.* **14**, 9556–9580 <https://doi.org/10.3390/ijms14059556>
- 82 Wang, S.Y. and Jiao, H. (2001) Changes in oxygen-scavenging systems and membrane lipid peroxidation during maturation and ripening in blackberry. *J. Agric. Food Chem.* **49**, 1612–1619 <https://doi.org/10.1021/jf0013757>

- 83 Jiménez, A., Creissen, G., Kular, B., Firmin, J., Robinson, S., Verhoeven, M. et al. (2002) Changes in oxidative processes and components of the antioxidant system during tomato fruit ripening. *Planta* **214**, 751–758 <https://doi.org/10.1007/s004250100667>
- 84 Zuccarelli, R., Rodríguez-Ruiz, M., Lopes-Oliveira, P.J., Pascoal, G.B., Andrade, S.C.S., Furlan, C.M. et al. (2021) Multifaceted roles of nitric oxide in tomato fruit ripening: NO-induced metabolic rewiring and consequences for fruit quality traits. *J. Exp. Bot.* **72**, 941–958 <https://doi.org/10.1093/jxb/eraa526>
- 85 Mondal, K., Malhotra, S.P., Jain, V. and Singh, R. (2009) Oxidative stress and antioxidant systems in Guava (*Psidium guajava* L.) fruits during ripening. *Physiol. Mol. Biol. Plants* **15**, 327–334 <https://doi.org/10.1007/s12298-009-0037-3>
- 86 Razzaq, K., Khan, A.S., Malik, A.U. and Shahid, M. (2013) Ripening period influences fruit softening and antioxidative system of 'Samar Bahisht Chaunsa' mango. *Sci. Hortic.* **160**, 108–114 <https://doi.org/10.1016/j.scienta.2013.05.018>
- 87 Nayab, S., Razzaq, K., Ullah, S., Rajwana, I.A., Amin, M., Faried, H.N. et al. (2020) Genotypes and harvest maturity influence the nutritional fruit quality of mulberry. *Sci. Hortic.* **266**, 109311 <https://doi.org/10.1016/j.scienta.2020.109311>
- 88 López-Huertas, E. and Palma, J.M. (2020) Changes in glutathione, ascorbate, and antioxidant enzymes during olive fruit ripening. *J. Agric. Food Chem.* **68**, 12221–12228 <https://doi.org/10.1021/acs.jafc.0c04789>
- 89 Endo, H. and Imahori, Y. (2016) Changes in hydrogen peroxide and superoxide anion contents and superoxide dismutase activity during the maturation of sweet pepper (*Capsicum annuum* L.) fruit. *Acta Hortic.* **1120**, 399–404 <https://doi.org/10.17660/ActaHortic.2016.1120.61>
- 90 Chu-Puga, Á., González-Gordo, S., Rodríguez-Ruiz, M., Palma, J.M. and Corpas, F.J. (2019) NADPH oxidase (Rboh) activity is up regulated during sweet pepper (*Capsicum annuum* L.) fruit ripening. *Antioxidants (Basel)* **8**, 9 <https://doi.org/10.3390/antiox8010009>
- 91 Guo, D.L., Wang, Z.G., Li, Q., Gu, S.C., Zhang, G.H. and Yu, Y.H. (2019) Hydrogen peroxide treatment promotes early ripening of Kyoho grape. *Aust. J. Grape Wine Res.* **25**, 357–362 <https://doi.org/10.1111/ajgw.12399>
- 92 Guo, D.-L., Wang, Z.-G., Pei, M.-S., Guo, L.-L. and Yu, Y.-H. (2020) Transcriptome analysis reveals mechanism of early ripening in Kyoho grape with hydrogen peroxide treatment. *BMC Genomics* **21**, 784 <https://doi.org/10.1186/s12864-020-07180-y>
- 93 Nene, T., Yadav, M. and Yadav, H.S. (2022) Plant catalase in silico characterization and phylogenetic analysis with structural modeling. *J. Genet. Eng. Biotechnol.* **20**, 125 <https://doi.org/10.1186/s43141-022-00404-6>
- 94 Ni, W. and Trelease, R.N. (1991) Post-transcriptional regulation of catalase isozyme expression in cotton seeds. *Plant Cell* **3**, 737–744 <https://doi.org/10.1105/tpc.3.7.737>
- 95 Ghorbel, M., Haddaji, N., Feki, K., Tounsi, S., Chihaoui, M., Alghamdi, A. et al. (2023) Identification of a putative kinase interacting domain in the durum wheat catalase 1 (TdCAT1) protein. *Heliyon* **9**, e18916 <https://doi.org/10.1016/j.heliyon.2023.e18916>
- 96 Zou, J.-J., Li, X.-D., Ratnasekera, D., Wang, C., Liu, W.-X., Song, L.-F. et al. (2015) Arabidopsis CALCIUM-DEPENDENT PROTEIN KINASE8 and CATALASE3 function in abscisic acid-mediated signaling and H₂O₂ homeostasis in stomatal guard cells under drought stress. *Plant Cell* **27**, 1445–1460 <https://doi.org/10.1105/tpc.15.00144>
- 97 Zhou, Y.-B., Liu, C., Tang, D.-Y., Yan, L., Wang, D., Yang, Y.-Z. et al. (2018) The receptor-like cytoplasmic kinase STRK1 phosphorylates and activates CatC, thereby regulating H₂O₂ homeostasis and improving salt tolerance in rice. *Plant Cell* **30**, 1100–1118 <https://doi.org/10.1105/tpc.17.01000>
- 98 Liu, C., Lin, J.-Z., Wang, Y., Tian, Y., Zheng, H.-P., Zhou, Z.-K. et al. (2023) The protein phosphatase PC1 dephosphorylates and deactivates CatC to negatively regulate H₂O₂ homeostasis and salt tolerance in rice. *Plant Cell* **35**, 3604–3625 <https://doi.org/10.1093/plcell/koad167>
- 99 Kirkman, H.N. and Gaetani, G.F. (1984) Catalase: a tetrameric enzyme with four tightly bound molecules of NADPH. *Proc. Natl Acad. Sci. U.S.A.* **81**, 4343–4347 <https://doi.org/10.1073/pnas.81.14.4343>
- 100 Kirkman, H.N. and Gaetani, G.F. (2007) Mammalian catalase: a venerable enzyme with new mysteries. *Trends Biochem. Sci.* **32**, 44–50 <https://doi.org/10.1016/j.tibs.2006.11.003>
- 101 Kirkman, H.N., Rolfo, M., Ferraris, A.M. and Gaetani, G.F. (1999) Mechanisms of protection of catalase by NADPH. Kinetics and stoichiometry. *J. Biol. Chem.* **274**, 13908–13914 <https://doi.org/10.1074/jbc.274.20.13908>
- 102 Clark, D., Durner, J., Navarre, D.A. and Klessig, D.F. (2000) Nitric oxide inhibition of tobacco catalase and ascorbate peroxidase. *Mol. Plant Microbe Interact.* **13**, 1380–1384 <https://doi.org/10.1094/MPMI.2000.13.12.1380>
- 103 Begara-Morales, J.C., Chaki, M., Sánchez-Calvo, B., Mata-Pérez, C., Leterrier, M., Palma, J.M. et al. (2013) Protein tyrosine nitration in pea roots during development and on activity stains for catalase. *J. Exp. Bot.* **64**, 1121–1134 <https://doi.org/10.1093/jxb/ert006>
- 104 Li, J., Shi, C., Wang, X., Liu, C., Ding, X., Ma, P. et al. (2020) Hydrogen sulfide regulates the activity of antioxidant enzymes through persulfidation and improves the resistance of tomato seedling to Copper Oxide nanoparticles (CuO NPs)-induced oxidative stress. *Plant Physiol. Biochem.* **156**, 257–266 <https://doi.org/10.1016/j.plaphy.2020.09.020>
- 105 Corpas, F.J., Barroso, J.B., González-Gordo, S., Muñoz-Vargas, M.A. and Palma, J.M. (2019) Hydrogen sulfide: a novel component in Arabidopsis peroxisomes which triggers catalase inhibition. *J. Integr. Plant Biol.* **61**, 871–883 <https://doi.org/10.1111/jipb.12779>
- 106 Palma, J.M., Ruiz, C. and Corpas, F.J. (2018) A simple and useful method to apply exogenous NO gas to plant systems: bell pepper fruits as a model. *Methods Mol. Biol.* **1747**, 3–11 https://doi.org/10.1007/978-1-4939-7695-9_1
- 107 Gayte, I.G., Moreno, R.B., Zonjic, P.S. and Claros, M.G. (2017) DEgenes Hunter - a flexible R pipeline for automated RNA-seq studies in organisms without reference genome. *Genomics Comput. Biol.* **3**, 31 <https://doi.org/10.18547/gcb.2017.vol3.iss3.e31>
- 108 Aebi, H. (1984) Catalase *in vitro*. *Methods Enzymol.* **105**, 121–126 [https://doi.org/10.1016/s0076-6879\(84\)05016-3](https://doi.org/10.1016/s0076-6879(84)05016-3)
- 109 Clare, D.A., Duong, M.N., Darr, D., Archibald, F. and Fridovich, I. (1984) Effects of molecular oxygen on detection of superoxide radical with nitroblue tetrazolium and on activity stains for catalase. *Anal Biochem.* **140**, 532–537 [https://doi.org/10.1016/0003-2697\(84\)90204-5](https://doi.org/10.1016/0003-2697(84)90204-5)
- 110 McGuffin, L.J., Atkins, J.D., Salehe, B.R., Shuid, A.N. and Roche, D.B. (2015) I-TFOLD: an integrated server for modelling protein structures and functions from amino acid sequences. *Nucleic Acids Res.* **43**, W169–W173 <https://doi.org/10.1093/nar/gkv236>
- 111 Fernandez-Fuentes, N., Madrid-Aliste, C.J., Rai, B.K., Fajardo, J.E. and Fiser, A. (2007) M4t: a comparative protein structure modeling server. *Nucleic Acids Res.* **35**, W363–W368 <https://doi.org/10.1093/nar/gkm341>
- 112 Kelley, L.A. and Sternberg, M.J.E. (2009) Protein structure prediction on the Web: a case study using the Phyre server. *Nat. Protoc.* **4**, 363–371 <https://doi.org/10.1038/nprot.2009.2>
- 113 Källberg, M., Wang, H., Wang, S., Peng, J., Wang, Z., Lu, H. et al. (2012) Template-based protein structure modeling using the RaptorX web server. *Nat. Protoc.* **7**, 1511–1522 <https://doi.org/10.1038/nprot.2012.085>

- 114 Arnold, K., Bordoli, L., Kopp, J. and Schwede, T. (2006) The SWISS-MODEL workspace: a web-based environment for protein structure homology modelling. *Bioinformatics* **22**, 195–201 <https://doi.org/10.1093/bioinformatics/bti770>
- 115 Varadi, M., Anyango, S., Deshpande, M., Nair, S., Natassia, C., Yordanova, G. et al. (2022) AlphaFold Protein Structure Database: massively expanding the structural coverage of protein-sequence space with high-accuracy models. *Nucleic Acids Res.* **50**, D439–D444 <https://doi.org/10.1093/nar/gkab1061>
- 116 Pettersen, E.F., Goddard, T.D., Huang, C.C., Couch, G.S., Greenblatt, D.M., Meng, E.C. et al. (2004) UCSF chimera—a visualization system for exploratory research and analysis. *J. Comput. Chem.* **25**, 1605–1612 <https://doi.org/10.1002/jcc.20084>
- 117 Laskowski, R.A., MacArthur, M.W., Moss, D.S. and Thornton, J.M. (1993) PROCHECK: a program to check the stereochemical quality of protein structures. *J. Appl. Crystallogr.* **26**, 283–291 <https://doi.org/10.1107/S0021889892009944>
- 118 Eisenberg, D., Lüthy, R. and Bowie, J.U. (1997) VERIFY3D: assessment of protein models with three-dimensional profiles. *Methods Enzymol.* **277**, 396–404 [https://doi.org/10.1016/s0076-6879\(97\)77022-8](https://doi.org/10.1016/s0076-6879(97)77022-8)
- 119 Colovos, C. and Yeates, T.O. (1993) Verification of protein structures: patterns of nonbonded atomic interactions. *Protein Sci.* **2**, 1511–1519 <https://doi.org/10.1002/pro.5560020916>
- 120 Vederas, J.C. and Floss, H.G. (1980) Stereochemistry of pyridoxal phosphate catalyzed enzyme reactions. *Acc. Chem. Res.* **13**, 455–463 <https://doi.org/10.1021/ar50156a004>
- 121 Chen, M., Zhang, W., Gou, Y., Xu, D., Wei, Y., Liu, D. et al. (2023) GPS 6.0: an updated server for prediction of kinase-specific phosphorylation sites in proteins. *Nucleic Acids Res.* **51**, W243–W250 <https://doi.org/10.1093/nar/gkad383>
- 122 Kabsch, W. and Sander, C. (1983) Dictionary of protein secondary structure: pattern recognition of hydrogen-bonded and geometrical features. *Biopolymers* **22**, 2577–2637 <https://doi.org/10.1002/bip.360221211>
- 123 Li, H., Robertson, A.D. and Jensen, J.H. (2005) Very fast empirical prediction and rationalization of protein pKa values. *Proteins* **61**, 704–721 <https://doi.org/10.1002/prot.20660>
- 124 Jurrus, E., Engel, D., Star, K., Monson, K., Brandi, J., Felberg, L.E. et al. (2018) Improvements to the APBS biomolecular solvation software suite. *Protein Sci.* **27**, 112–128 <https://doi.org/10.1002/pro.3280>
- 125 Krissinel, E. and Henrick, K. (2007) Inference of macromolecular assemblies from crystalline state. *J. Mol. Biol.* **372**, 774–797 <https://doi.org/10.1016/j.jmb.2007.05.022>